



Flexible molybdenum phosphide nanosheet array electrodes for hydrogen evolution reaction in a wide pH range

Zonghua Pu^a, Shiyong Wei^b, Zhibao Chen^b, Shichun Mu^{a,*}

^a State Key Laboratory of Advanced Technology for Materials Synthesis and Processing, Wuhan University of Technology, Wuhan 430070, China

^b Jiangxi Key Laboratory for Advanced Copper and Tungsten Materials, Jiangxi Academy of Sciences, Nanchang 330029, China

ARTICLE INFO

Article history:

Received 8 December 2015

Received in revised form 30 March 2016

Accepted 16 May 2016

Available online 17 May 2016

Keywords:

MoP nanosheets

Carbon cloth

Hydrogen evolution reaction

Electrocatalyst

All pH values

ABSTRACT

Searching for non-noble-metal hydrogen evolution reaction (HER) electrocatalysts with high efficiency and excellent durability is a great challenge for the hydrogen-based energy industry. In this paper, a three-dimensional self-supported hydrogen evolution cathode is present, where the MoP nanosheet array was grown on flexible carbon cloth (MoP NA/CC) via a two-step strategy: hydrothermally growing MoS₂ nanosheet array on CC (MoS₂ NA/CC) in advance, and then phosphidation to chemically convert the MoS₂ NA/CC precursor into MoP NA/CC. When used as an integrated three-dimensional electrode for HER, MoP NA/CC shows a quiet low onset overpotential (50 mV vs reversible hydrogen electrode), high current density ($j > 10 \text{ mA cm}^{-2}$ at $\eta = 124 \text{ mV}$), and a small Tafel slope (58 mV dec^{-1}), as well as remarkable stability ($< 9\%$ decay after 46 h electrolysis) in acidic conditions. Interestingly, the flexible MoP NA/CC electrode also offers superior electrocatalytic performance and remarkable durability for HER in both neutral and basic conditions.

© 2016 Elsevier B.V. All rights reserved.

1. Introduction

As an ideal clean fuel with outstanding energy storage density, hydrogen is considered as the most promising energy carrier in the future [1,2]. Water electrolysis is one of the easiest and cleanest routes to produce highly pure hydrogen through hydrogen evolution reaction (HER) [3]. Generally, HER is most effectively catalyzed by precious Pt-based materials, but the high expense and scarcity of Pt is not suitable for widespread use. The electrochemical water splitting system works well under strongly acidic (based on the proton exchange membrane (PEM) technology) [4], neutral (microbial electrolysis cell) [5], or strongly basic media (alkaline electrolysis) [6]. Therefore, the design of HER catalysts capable of operating efficiently over a wide pH range is highly desired but still remains challenging, and up to now only very limited success has been reported [7–11].

Molybdenum (Mo)-based materials, including MoS₂ [12–16], MoSe₂ [17], Mo₂C [18–20], MoB [20], MoN [21], NiMoN_x/C [22], Co_{0.6}Mo_{1.4}N₂ [23] and MoP [24–27], have been widely investigated for catalyzing the electrochemical HER owing to their low cost and superior catalytic activities. Among them, MoP is known for transition metal phosphide that has high electrical conductivity

and excellent HER catalytic activity under both acidic and alkaline media. Indeed, quantum chemical calculations have suggested that MoP can introduce a good “H delivery” system which attains nearly zero binding to H at certain coverage [27]. Recently, great effort has been spent on the structure and component design of MoP-based catalyst to further enhance the HER activity. For example, Xing et al. synthesised MoP nanoparticles with interconnected network structure, resulting in a high HER activity [24]. McEnaney et al. reported a discrete, uniform amorphous MoP nanoparticle, exhibiting a small Tafel slope (45 mV dec^{-1}) [25]. Cui et al. successfully synthesised MoP nanosheets grown on carbon flake by a one-step solid state reaction, which improved the conductivity and the final activity [26]. Also, Kibsgaard et al. presented a sulfidation treatment of MoP, and the prepared phosphosulfide surface (MoP₂S) led to a remarkable improvement in the catalyst performance [28]. Despite great efforts, prior to HER tests, such catalysts involves several steps, including mixing the active materials with polymer binders (such as Nafion), and then immobilizing the mixture on electrode surfaces. However, the utilization of electrical insulating polymer binder might decrease the electrical conductivity and block catalytic active sites as well as inhibit the diffusion channels of ion transportation, leading to reduced electrocatalytic performance [29,30]. The direct fabrication of catalyst films on current collectors for a binder-free hydrogen evolution cathode could avoid such problems [31–34]. Until recently, Yan and coworkers grew MoP nanoparticles on commercially sponges, exhibiting a

* Corresponding author.

E-mail addresses: msc@whut.edu.cn, mushichun@gmail.com (S. Mu).

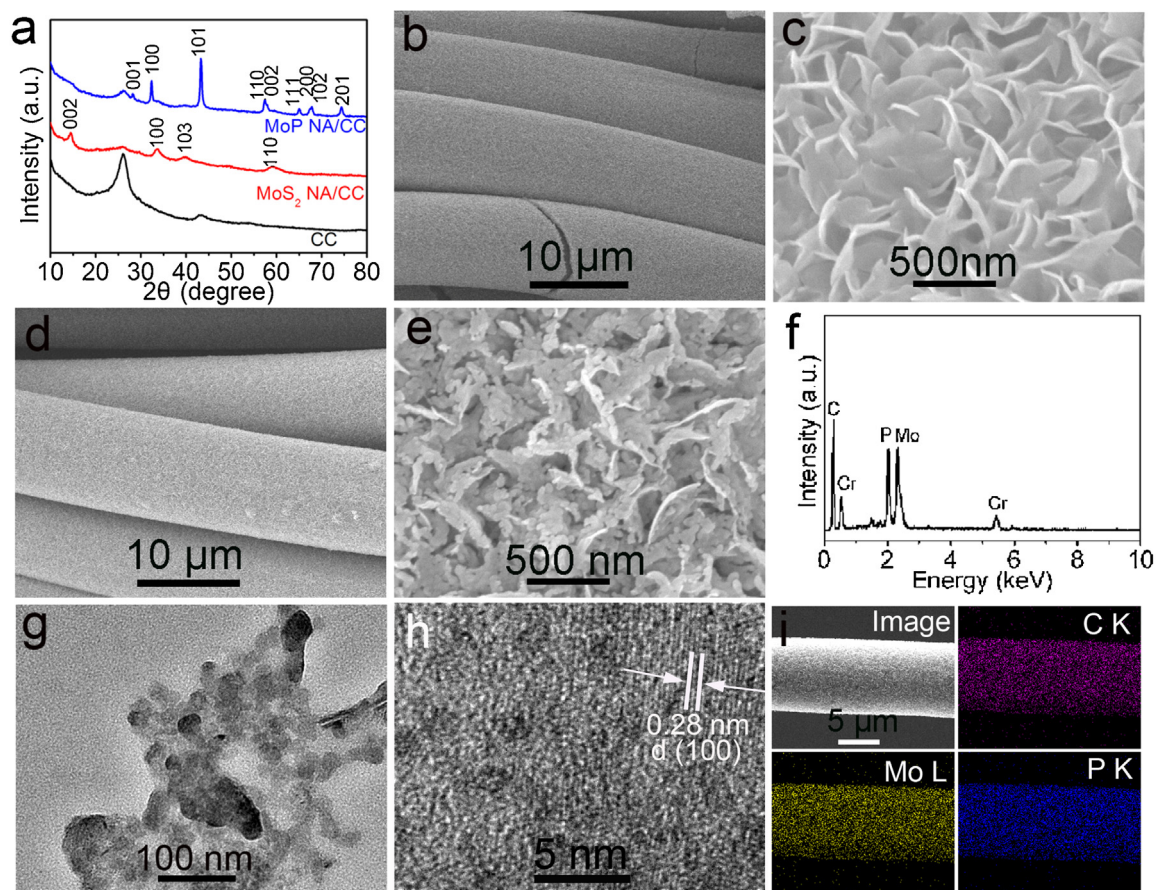


Fig. 1. (a) XRD patterns for CC, MoS₂ NA/CC and MoP NA/CC. (b) Low- and (c) high-magnification SEM images of MoS₂ NA/CC. (d) Low- and (e) high-magnification SEM images of MoP NA/CC. (f) EDX spectrum of MoP NA/CC. (g) TEM and (h) HRTEM image of MoP nanosheets. (i) SEM image and EDX elemental mapping of C, Mo and P for MoP NA/CC.

high HER activity. Unfortunately, this catalyst needs dangerous gas (H₂) for preparation and only the HER behaviour in acidic and basic media were studied [35]. To the best of our knowledge, no research has been paid to the MoP-integrated hydrogen evolution cathode efficiently over a wide pH range.

In this study, we firstly synthesize the MoP nanosheet array supported on highly flexible carbon cloth (MoP NA/CC) via a two-step process: hydrothermally growing MoS₂ nanosheet array on CC (MoS₂ NA/CC) first, followed by phosphidation to chemically convert the MoS₂ NA/CC precursor into MoP NA/CC. As an integrated three-dimensional hydrogen evolution electrode, MoP NA/CC exhibits excellent catalytic activity and durability under all pH values.

2. Experimental

2.1. Materials

Potassium hydroxide (KOH), potassium phosphate (KH₂PO₄, K₂HPO₄), sodium hypophosphite (NaH₂PO₂·H₂O) and ethanol were purchased from Aladdin Reagent. Sulfuric acid (H₂SO₄) and red phosphorus were purchased from Beijing Chemical Works. Sodium molybdate (Na₂MoO₄·2H₂O) and thiourea were purchased from Xinglong Chemical Corp. Nafion (5 wt%) and Pt/C (20 wt%) were purchased from Sigma-Aldrich. All the reagents in the experiment were analytical grade and without further treatments. Deionized Mini-Q water was used as solvent.

2.2. Preparation of MoS₂ NA/CC and MoP NA/CC

Firstly, CC was cleared by ultrasonic with ethanol and water. In brief, 4 mmol Na₂MoO₄·2H₂O and 8 mmol thiourea were dissolved in 60 mL deionized H₂O. Then, the solution was transferred into a 100 mL Teflon-lined stainless steel autoclave. A piece of CC (2 × 4 cm²) was vertically inserted into the above solution, and the autoclave was heated at 200 °C for 18 h. After cooling, the as synthesized product was washed with plenty of water and dried at 60 °C overnight. To obtain MoP NA/CC, the as-prepared MoS₂ NA/CC and red phosphorus were put into a porcelain boat (P to Mo is 5:1) and annealed at 800 °C under N₂ atmosphere for 1 h. The loading of MoP on CC was about 2.5 mg cm⁻².

2.3. Characterizations

X-ray diffraction (XRD) patterns were collected on a Rigaku X-ray diffractometer equipped with a Cu K α radiation source. The morphology and structure were characterized by scanning electron microscopy (SEM, XL30 ESEM FEG) and transmission electron microscopy (TEM, HITACHI H-8100). X-ray photoelectron spectroscopy (XPS) was obtained on an ESCALABMK II X-ray photoelectron spectrometer.

2.4. Electrochemical measurements

The electrochemical tests for HER were carried out with a CHI 660E electrochemical workstation using a three-electrode configuration with as-prepared electrodes, the Ag/AgCl (3.0 M

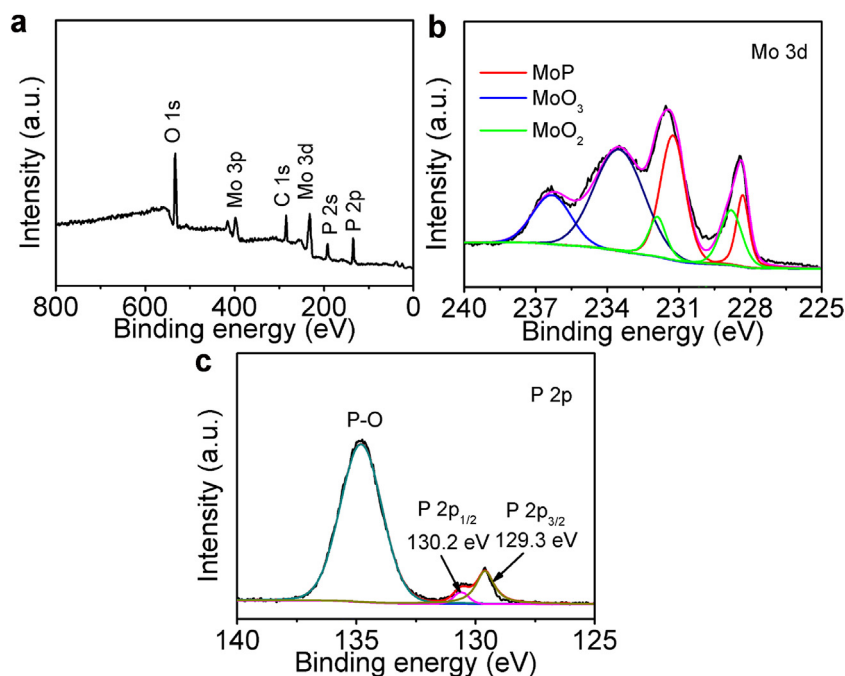


Fig. 2. (a) XPS survey spectrum for MoP NA/CC. XPS spectra in the (b) Mo 3d and (c) P 2p regions for MoP NA/CC.

KCl) and graphite rod as the working electrode, reference electrode and auxiliary electrode, respectively. The polarization curves were recorded in 0.5 M H_2SO_4 (pH=0), 1.0 M phosphate buffered solution (PBS, pH=7.0) and 1.0 M KOH (pH=14) with a scan rate of 2 mV s^{-1} at room temperature ($\sim 25^\circ\text{C}$), respectively. The measured potentials vs. Ag/AgCl were converted to a reversible hydrogen electrode (RHE) scale. In 0.5 M H_2SO_4 , $E_{\text{RHE}} = E_{\text{Ag/AgCl}} + 0.197 \text{ V}$, In 1.0 M PBS, $E_{\text{RHE}} = E_{\text{Ag/AgCl}} + 0.610 \text{ V}$, In 1.0 M KOH, $E_{\text{RHE}} = E_{\text{Ag/AgCl}} + 1.023 \text{ V}$. Electrochemical impedance spectroscopy (EIS) measurements were performed in the frequency from 1 kHz to 100 Hz under the amplitude of 5 mV. To reflect the real catalytic currents, all polarization curves were corrected for the iR loss and the background current.

3. Results and discussion

The prepared MoP NA/CC represents a high flexibility and can even endure folding and twisting without destroying its construction (Fig. S1). Owing to its high flexibility, MoP NA/CC exhibits potential applications for flexible energy conversion systems, such as shape conformability, light weight, small unit, which enable their applications in foldable, bendable, portable and even wearable devices [36]. XRD was used for phase identification (Fig. 1a). MoS_2 NA/CC shows a diffraction characteristic peak of hexagonal-phase MoS_2 (JCPDS No. 65-0160). After a phosphidation treatment, most of the characteristic peaks can be indexed to MoP (JCPDS No. 24-0771) [37]. The remaining two peaks at 26° and 43° are ascribed to the CC substrate. SEM images of the bare CC (Fig. S2) indicate it consists of smooth microfibers with an average diameter of about $10 \mu\text{m}$. Fig. 1b and c shows a three-dimensional open porous structure of MoS_2 NA/CC, and each nanosheet is interconnected with each other to form nanosheet arrays. It is noted that the phosphidated products still maintain the nanosheet feature but with rough surfaces, which is clearly evidenced by their SEM images (Fig. 1d and e). Energy dispersive X-ray (EDX) spectrum (Fig. 1f) verifies the presence of elemental P and Mo (other peaks come from the CC substrate and sputtered Cr used for SEM characterization) and the atomic ratio between P and Mo is close to 1:1. Fig. 1g shows the TEM image of MoP nanosheets consisted of MoP nanoparticles. A rep-

resentative high-resolution TEM (HRTEM) image (Fig. 1h) clearly exhibits well-defined lattice fringes with an interplane spacing of 0.28 nm, which can be indexed to the (100) plane of MoP. SEM image and EDX elemental mapping images (Fig. 1i) verify that all elements (C, P and Mo) in MoP NA/CC are uniformly distributed in the whole microfiber. All these observations confirm the successful chemical conversion of MoS_2 NA/CC into MoP NA/CC after the phosphidation reaction.

XPS analysis was performed to elucidate the valence states of Mo and P in MoP NA/CC. The XPS survey spectrum (Fig. 2a) indicates that the presence of O, P and Mo elements, and elemental O could be attributed to surface oxidation of MoP NA/CC due to the possible air contact. Fig. 2b and c presents the high-resolution XPS spectra of Mo 3d and P 2p. The binding energies of Mo $3d_{5/2}$ and Mo $3d_{3/2}$ at 228.3 and 231.2 eV can be assigned to $\text{Mo}^{\delta+}$ species ($0 < \delta < 4$), which are typical peaks for MoP [38,39]. Other Mo $3d_{3/2}$ and Mo $3d_{5/2}$ binding energies at 231.8 and 228.7 eV for Mo^{4+} , 233.4 and 236.3 eV for Mo^{6+} , can be assigned to MoO_2 and MoO_3 , respectively [40,41]. It has been reported that the surface of MoP can be readily contaminated with molybdenum oxides when exposed to air [27]. The high-resolution spectrum of P 2p shows two peaks at 129.3 and 130.2 eV corresponding to the binding energy of P $2p_{3/2}$ and P $2p_{1/2}$ as well as a peak at 134.3 eV [37,42]. The predominant P species on the catalyst surface with a P $2p_{3/2}$ binding energy of 129.3 eV are assigned to P bonded to Mo, while the peak at 134.3 eV could be due to surface PO_4^{3-} or P_2O_5 species when the catalyst was exposed to air [27,37]. These analyses suggest the success formation of MoP nanosheets.

Fig. 3a and b shows the polarization curves with a scan rate of 2 mV s^{-1} in H_2 -saturated 0.5 M H_2SO_4 after iR-compensation for MoP NA/CC and MoS_2 NA/CC. Commercial 20 wt% Pt/C and bare CC are also examined for comparison. Pt/C shows an excellent HER performance with negligible overpotentials, while bare CC has a very limited HER activity. It is noted that MoS_2 NA/CC exhibits an intrinsic catalytic activity toward HER with an onset overpotential of 72 mV. In stark contrast, MoP NA/CC shows a smaller onset overpotential of 50 mV. In addition, the overpotentials required to drive the current densities of 10 and 100 mA cm^{-2} are 124 and 176 mV for

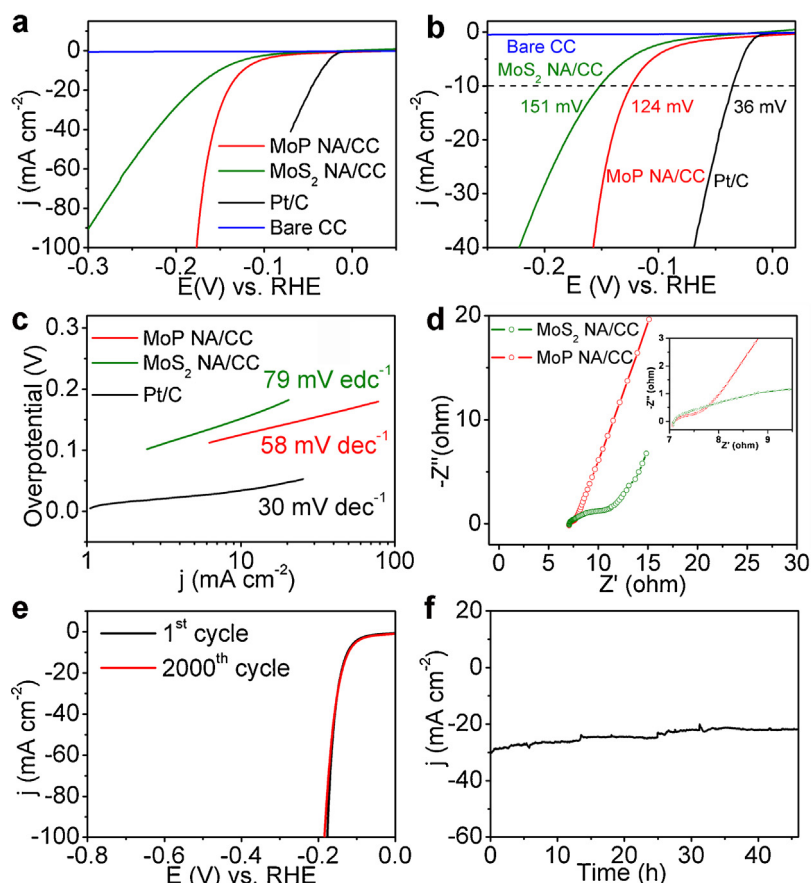


Fig. 3. (a, b) Polarization curves of MoS₂ NA/CC, Pt/C, MoP NA/CC and bare CC in 0.5 M H₂SO₄ with a scan rate of 2 mV s⁻¹. (c) Tafel plots of MoS₂ NA/CC, MoP NA/CC and Pt/C. (d) Nyquist plots of MoP NA and MoS₂ NA/CC recorded at 0.28 V vs. RHE in 0.5 M H₂SO₄. (e) Polarization curves recorded for MoP NA/CC before and after 2000 CV cycles. (f) Time-dependent current density curve for MoP NA/CC under static overpotential of 150 mV for 46 h.

MoP NA/CC, respectively. Table S1 lists HER activity parameters of Mo-based HER catalysts in acidic media. Strikingly, our developed MoP NA/CC shows a high activity comparable with other catalysts.

To study the electrocatalytic kinetics of HER, corresponding Tafel slopes were derived from chronoamperometric measurements, as shown in Fig. 3c. The Tafel slope for Pt/C is 30 mV dec⁻¹ [43–45], while MoP NA/CC exhibits a smaller Tafel slope (58 mV dec⁻¹) than that of MoS₂ NA/CC (79 mV dec⁻¹). The values of the Tafel slopes suggest that HER of both catalysts occurs via a Volmer-Heyrovsky mechanism [21,46]. Moreover, by extrapolating the Tafel plot, the exchange current density (j_0) of MoP NA/CC is 0.13 mA cm⁻² (Fig. S3). This value is much higher than those reported MoP-based catalysts such as MoP interconnected network nanoparticles (0.086 mA cm⁻²) [24], amorphous MoP nanoparticles (0.12 mA cm⁻²) [25], MoP nanoparticles (0.034 mA cm⁻²) [27]. To illustrate the electrode kinetics for MoP NA/CC, the EIS data of MoP NA/CC and MoS₂ NA/CC are shown in Fig. 3d. Nyquist plots and data fittings to a simplified equivalent circuit (Fig. S4) reveal that the charge transfer resistance (R_{ct}) value of MoP NA/CC (65.6 Ω) is much lower than MoS₂ NA/CC (1299 Ω) (Table S2). This result suggests that MoP NA/CC has better electronic conductivity than that of MoS₂ NA/CC, which leads to a highly efficient electron transport and favourable HER kinetics at the MoP nanosheets/electrolyte interfaces [47].

For real applications the corrosion durability is another critical factor for evaluating a HER catalyst. Therefore, the accelerated stability tests of the MoP NA/CC catalyst were probed via continuous cyclic voltammetric (CV) sweeping at a scan rate of 100 mV s⁻¹. After 2000 cycle, no change in the polarization curve of MoP NA/CC

is observed (Fig. 3e), indicating the stable HER electrocatalysis of the material in acid. The long-term durability of this catalyst was also evaluated by electrolysis at $\eta = 150$ mV, suggesting 91% of the current density was maintained after electrolysis for more than 46 h (Fig. 3f). These results confirm the excellent durability of MoP NA/CC for HER.

Next, the catalyst activity of MoP NA/CC was further investigated in both neutral and basic media. As shown in Fig. 4a and d, the MoP NA/CC exhibits excellent HER activity in 1.0 M PBS (pH = 7) and 1.0 M KOH (pH = 14). The overpotentials of 187 and 80 mV are needed to driving a current density of 10 mA cm⁻² in pH = 7 and 14, respectively. Likewise, when the HER current density reaches 100 mA cm⁻², the overpotential require 379 and 181 mV, respectively. The Tafel slope of MoP NA/CC is 94 mV dec⁻¹ in pH = 7 and 83 mV dec⁻¹ in pH = 14 (Fig. 4b and e). In addition, MoP NA/CC also shows strong durability in both media (Fig. 4c and f). It is worth noting that MoP NA/CC shows comparable catalytic activities to the most reported Pt-free HER catalysts in neutral or basic solutions (Table S3 and S4).

Such superior catalytic activity and stability of MoP NA/CC than most of conventional catalysts can be ascribed to following facts: First, generally speaking, conventional catalysts are prepared in the form of one-dimensional (1D) or 2D structure, and randomly aggregated when preparing electrodes for HER tests. Such disordered aggregates not only inhibit diffusion, but also block the active sites, leading to reduced electrocatalytic performance. Thus, a 3D porous structure of MoP NA/CC contributes to attain high catalytic performance by facilitating the reaction kinetic in the channel-rich structure. Second, the 3D porous structure ensures

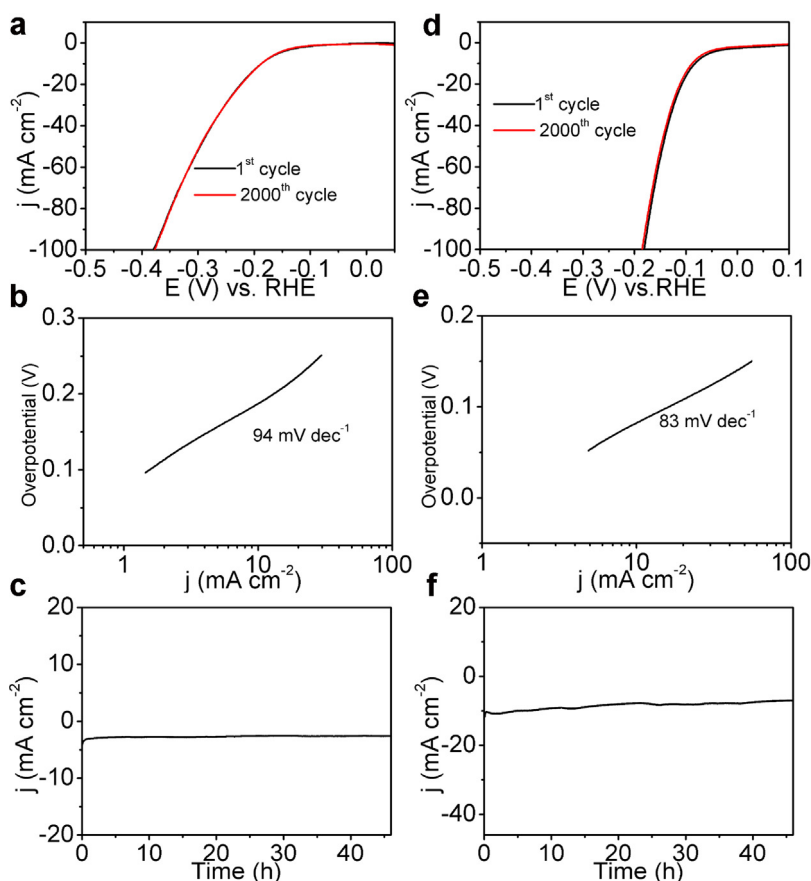


Fig. 4. Polarization curves, Tafel plot and time-dependent current density curve for MoP NA/CC in (a–c) 1.0 M PBS and (d–f) 1.0 M KOH.

easy contact of much more surfaces with the electrolyte and more exposed active sites to facilitate the hydrogen production process. Third, as reported, Mo acts as the hydride-acceptor and P acts as proton-acceptor center, facilitating the HER catalytic activity [48]. In addition, the direct anchoring of MoP NA on conductive CC guarantees good durability of the catalyst during the long-term operation.

4. Conclusion

In summary, we report a two-step strategy for controllable synthesis of a MoP nanosheet array on flexible carbon cloth. As a novel three-dimensional cathode for catalyzing the HER, this electrode exhibits excellent electrocatalytic activity and durability at all pH conditions. The facile and low-cost synthesis, together with its high catalytic activity and long-term electrochemical durability of this flexible three-dimensional electrode, promises its large-scale application toward scalable electrochemical hydrogen production from water.

Acknowledgements

This work was supported by the National Natural Science Foundation of China (51372186), and the open Foundation of Jiangxi Key Laboratory of Advanced Copper and Tungsten Materials (2013-KLP-05).

Appendix A. Supplementary data

Supplementary data associated with this article can be found, in the online version, at <http://dx.doi.org/10.1016/j.apcatb.2016.05.027>.

References

- [1] M.S. Dresselhaus, I.L. Thomas, *Nature* 414 (2001) 332–337.
- [2] S. Gu, B. Xu, Y. Yan, *Annu. Rev. Chem. Biomol. Eng.* 5 (2014) 429–454.
- [3] M.G. Walter, E.L. Warren, J.R. McKone, S.W. Boettcher, Q.X. Mi, E.A. Santori, N.S. Lewis, *Chem. Rev.* 10 (2010) 6446–6473.
- [4] A.L. Goff, V. Artero, B. Josselme, P.D. Tran, N. Guillet, R. Métayé, A. Fihri, S. Palacin, M. Fontecave, *Science* 326 (2009) 1384–1387.
- [5] A. Kundu, J.N. Sahu, G. Redzwan, M.A. Hashim, *Int. J. Hydrogen Energy* 38 (2013) 1745–1757.
- [6] R.L. LeRoy, *Int. J. Hydrogen Energy* 8 (1983) 401–417.
- [7] S. Gao, G. Li, Y. Liu, H. Chen, L. Feng, Y. Wang, M. Yang, D. Wang, S. Wang, X. Zou, *Nanoscale* 7 (2015) 2306–2316.
- [8] X. Zou, X. Huang, A. Goswami, R. Silva, B.R. Sathe, E. Mikmekova, T. Asefa, *Angew. Chem. Int. Ed.* 126 (2014) 4461–4465.
- [9] Z. Pu, Q. Liu, A.M. Asiri, X. Sun, *ACS Appl. Mater. Interfaces* 6 (2014) 21874–21879.
- [10] Z. Pu, Q. Liu, A.M. Asiri, X. Sun, *Electrochim. Acta* 168 (2015) 133–138.
- [11] Y. Liu, G. Yu, G. Li, Y. Sun, T. Asefa, W. Chen, X. Zou, *Angew. Chem. Int. Ed.* 54 (2015) 10752–10757.
- [12] T.F. Jaramillo, K.P. Jorgensen, J. Bonde, J.H. Nielsen, S. Hørch, I. Chorkendorff, *Science* 317 (2007) 100–102.
- [13] Z. Chen, D. Cummins, B.N. Reinecke, E. Clark, M.K. Sunkara, T.F. Jaramillo, *Nano Lett.* 11 (2011) 4168–4175.
- [14] Y. Hou, B. Zhang, Z.H. Wen, S.M. Cui, X.R. Guo, Z. He, J.H. Chen, *J. Mater. Chem. A* 2 (2014) 13795–13800.
- [15] J. Kibsgaard, Z. Chen, B.N. Reinecke, T.F. Jaramillo, *Nat. Mater.* 11 (2012) 963–969.
- [16] J. Deng, H. Li, J. Xiao, Y. Tu, D. Deng, H. Yang, H. Tian, J. Li, P. Ren, X. Bao, *Energy Environ. Sci.* 8 (2015) 1594–1601.
- [17] D. Kong, H. Wang, J.J. Cha, M. Past, K.J. Koski, J. Yao, Y. Cui, *Nano Lett.* 13 (2013) 1341–1347.

- [18] W. Chen, C. Wang, K. Sasaki, N. Marinkovic, W. Xu, J.T. Muckerman, Y. Zhu, R.R. Adzic, *Energy Environ. Sci.* 6 (2013) 943–951.
- [19] L. Liao, S. Wang, J. Xiao, X. Bian, Y. Zhang, M.D. Scanlon, X. Hu, Y. Tang, B. Liu, H.H. Girault, *Energy Environ. Sci.* 7 (2014) 387–392.
- [20] H. Vrubel, X. Hu, *Angew. Chem. Int. Ed.* 51 (2012) 12703–12706.
- [21] W.F. Chen, J.T. Muckerman, E. Fujita, *Chem. Commun.* 49 (2013) 8896–8909.
- [22] W.F. Chen, K. Sasaki, C. Ma, A.I. Frenkel, N. Marinkovic, J.T. Muckerman, Y. Zhu, R.R. Adzic, *Angew. Chem. Int. Ed.* 51 (2012) 6131–6135.
- [23] B. Cao, G.M. Veith, J.C. Neuefeind, R.R. Adzic, P.G. Khalifah, *J. Am. Chem. Soc.* 135 (2013) 19186–19192.
- [24] Z. Xing, Q. Liu, A.M. Asiri, X. Sun, *Adv. Mater.* 26 (2014) 5702–5707.
- [25] J.M. McEnaney, J.C. Crompton, J.F. Callejas, E.J. Popczun, A.J. Biacchi, N.S. Lewis, R.E. Schaak, *Chem. Mater.* 26 (2014) 4826–4831.
- [26] W. Cui, Q. Liu, Z. Xing, A.M. Asiri, K.A. Alamry, X. Sun, *Appl. Catal. B—Environ.* 164 (2015) 144–150.
- [27] P. Xiao, M.A. Sk, L. Thia, X. Ge, R.J. Lim, J.Y. Wang, K.H. Lim, X. Wang, *Energy Environ. Sci.* 7 (2014) 2624–2629.
- [28] J. Kibsgaard, T.F. Jaramillo, *Angew. Chem. Int. Ed.* 53 (2014) 14433–14437.
- [29] Y. Luo, J. Jiang, W. Zhou, H. Yang, J. Luo, X. Qi, H. Zhang, D.Y.W. Yu, C.M. Li, T. Yu, *J. Mater. Chem.* 22 (2012) 8634–8640.
- [30] J.D. Roy-Mayhew, G. Boschloo, A. Hagfeldt, I.A. Aksay, *ACS Appl. Mater. Interfaces* 4 (2012) 2794–2800.
- [31] W. Zhou, Y. Zhou, L. Yang, J. Huang, Y. Ke, K. Zhou, L. Li, S. Chen, *J. Mater. Chem. A* 3 (2015) 1915–1919.
- [32] P. Jiang, Q. Liu, Y. Liang, J. Tian, A.M. Asiri, X. Sun, *Angew. Chem. Int. Ed.* 53 (2014) 12855–12859.
- [33] Z. Pu, Q. Liu, P. Jiang, A.M. Asiri, A.Y. Obaid, X. Sun, *Chem. Mater.* 26 (2014) 4326–4329.
- [34] Z. Pu, Q. Liu, C. Tang, A.M. Asiri, X. Sun, *Nanoscale* 6 (2014) 11031–11034.
- [35] C. Deng, F. Ding, X. Li, Y. Guo, W. Ni, H. Yan, K. Sun, Y. Yan, *J. Mater. Chem. A* 4 (2016) 59–66.
- [36] T. Ma, J. Ran, S. Dai, M. Jaroniec, S. Qiao, *Angew. Chem. Int. Ed.* 54 (2015) 4646–4650.
- [37] X. Chen, D. Wang, Z. Wang, P. Zhou, Z. Wu, F. Jiang, *Chem. Commun.* 50 (2014) 11683–11686.
- [38] J. Bai, X. Li, A. Wang, R. Prins, Y. Wang, *J. Catal.* 287 (2012) 161–169.
- [39] D.C. Phillips, S.J. Sawhill, R. Self, M.E. Bussell, *J. Catal.* 207 (2002) 266–273.
- [40] X. Zhao, M. Cao, B. Liu, Y. Tian, C. Hu, *J. Mater. Chem.* 22 (2012) 13334–13340.
- [41] O.G. Marin Flores, S. Ha, *Appl. Catal. A Gen.* 352 (2009) 124–132.
- [42] A.P. Grosvenor, S.D. Wik, R.G. Cavell, A. Mar, *Inorg. Chem.* 44 (2005) 8988–8998.
- [43] E.J. Popczun, J.R. McKone, C.G. Read, A.J. Biacchi, A.M. Wiltrout, N.S. Lewis, R.E. Schaak, *J. Am. Chem. Soc.* 135 (2013) 9267–9270.
- [44] E.J. Popczun, C.G. Read, C.W. Roske, N.S. Lewis, R.E. Schaak, *Angew. Chem. Int. Ed.* 126 (2014) 5431–5534.
- [45] J.M. McEnaney, J.C. Crompton, J.F. Calleja, E.J. Popczun, C.G. Read, N.S. Lewis, R.E. Schaak, *Chem. Commun.* 50 (2014) 11026–11028.
- [46] B.E. Conway, B.V. Tilak, *Electrochim. Acta* 47 (2002) 3571–3594.
- [47] P. Xiao, Y. Yan, X. Ge, Z. Liu, J. Wang, X. Wang, *Appl. Catal. B—Environ.* 154 (2014) 232–237.
- [48] P. Liu, J.A. Rodriguez, *J. Am. Chem. Soc.* 127 (2005) 14871–14878.